Materials Research Proceedings 35 (2023) 241-248 https://doi.org/10.21741/9781644902714-29

Ductility and linear energy density of Ti6Al4V parts produced with additive powder bed fusion technology

Gianluca Buffa[1,a *], Dina Palmeri[1,b], Gaetano Pollara[1,c], Livan Fratini[1,d], Alessandro Benigno[2,e],

[1]Dipartimento di Ingegneria, Università degli Studi di Palermo, Viale delle Scienze 90128, Palermo, Italy

[2]AB Ingegneria, Via Segesta 26, 90141, Palermo, Italy

[a] gianluca.buffa@unipa.it, [b] dina.palmeri@unipa.it, [c] gaetano.pollara@unipa.it, [d] livan.fratini@unipa.it, [e] alessandrobenigno@libero.it

Keywords: Powder Bed Fusion, Linear Energy Density, Ductility

Abstract. Hybrid metal forming processes involve the integration of commonly used sheet metal forming processes, as bending, deep drawing and incremental forming, with additive manufacturing processes as Powder Bed Fusion. In recent ybears, these integrations have been more developed for manufacturing sectors characterized by components with complex geometries in low numbers, as the aerospace sector. Hybrid additive manufacturing overcomes the typical limitations of additive manufacturing related to low productivity, metallurgical defects and low dimensional accuracy. In this perspective, a key aspect of hybrid processes is the production of parts characterized by high strength and ductility. In the present work, a study was carried out on the influence of process parameters, such as laser power and scanning speed, on material ductility for Ti6Al4V alloy samples produced by Selective Laser Melting. In particular, the material strength and ductility were related to the process linear energy density (LED).

Introduction

Recently, there has been a rise in interest in additive manufacturing (AM) technologies due to their capacity to produce complex shapes. Changes to the part designs can be rapidly and readily incorporated using this technique. Moreover, because no tooling is required, production time is decreased in general [1]. With AM techniques, less process scrap is generated as a three-dimensional component is built layer by layer from the material in the form of wire or powder [2]. It is advisable to use forming procedures that offer quicker production periods when producing large batch sizes due to AM's slow rate of production. Moreover, the use of additive manufacturing (AM) in tight-tolerance and critical applications is constrained by its low resolution, the occurrence of porosity defects, partially melted powder, and residual tensions [3]. Unfortunately, forming procedures are not versatile enough to produce a variety of product variants since they require specific instruments [4].

Due to the possibility to use the unique advantages of each technique to improve part qualities above conventional production, hybrid techniques have become more and more common as a means of overcoming these restrictions. Incorporating more materials, structures, or functionalities into the component is made possible by combining additive manufacturing with other traditional methods, leading to improved new attributes. Economic aspects may be enhanced together with technical benefits. In terms of L-PBF and forming, AM makes it possible to do away with the requirement for a single forming machine configuration for the creation of pre-forms and a single forming tool that needs to be designed for each part geometry [5].

Several process chains have recently been researched with a focus on titanium alloys. In comparison to ordinary wrought material with a lamellar microstructure generally used in the

Materials Research Proceedings 35 (2023) 241-248 https://doi.org/10.21741/9781644902714-29

traditional forging of Ti-6Al-4V, it has been demonstrated that AM materials display good formability, lower flow stresses, and activation energy for hot forming [6]. It's crucial to ensure that the printed pieces can withstand the generated distortion before carrying out the subsequent forming procedure. Hence, the paper's goal is to provide a production window to create components with increased ductility and strength for use in the hybrid forming process. The effects of building orientation on the mechanical characteristics of titanium alloy generated by casting, selective laser melting (SLM), and electron beam melting were investigated by Pasang et al (EBM). With the exception of 45° orientation, when SLM samples displayed greater strength, wrought samples produced the greatest results.

The ductility of the wrought alloy consistently outperformed that of SLM and EBM [7]. Surface morphology was chosen by Wang et al. as the quality indicator for SLM parts. They established a relationship between the line energy density and the manufactured samples' surface quality, which influences their ductility [8]. One of the causes of the brittle fractures of selectively melted Ti6Al4V, according to Moridi et al., is the existence of printing flaws during the process [9]. Liu et al. investigated the impact of the process parameters to enhance the printed parts' tensile strength and ductility. It was found that the process parameters have a significant impact on the tensile behaviour, in particular the ductility, of the Ti alloy created by SLM. The significant improvement in mechanical behaviour is principally attributable to the decrease of pores and the limiting of martensite production [10]. In order to reduce these flaws and increase ductility, process parameter optimization is crucial. In the present work, a study was carried out on the influence of process parameters, such as laser power and scanning speed, on material ductility for Ti6Al4V alloy samples produced by Selective Laser Melting. In particular, the material strength and ductility were related to the process linear energy density (LED).

Materials and Method

Ti6Al4V powder with a particle size of 20-60 μm was used in this study. All of the samples were created using the L-PBF process by the SLM 280 HL machine. Argon inert gas was used to completely fill the printing chamber and lower the oxygen content to less than 0.1%. To minimize pore defects and increase the strength of the material, the building orientation was maintained constant and set at 0° [11, 12]. In order to examine the impact of line energy density (LED) on the ductility of the printed parts, hatch distance, layer thickness, and scan strategy were also kept constant at 100 μm, 60 μm, and 0°, respectively. In particular, 39 samples (N=3 duplicates for set of parameters) with varying LED levels between 0,175 and 0,258 J/mm were produced.

The selection of the LED values has been conducted without a uniform increase in order to have more data near the LED value suggested by SLM solution equal to 0,25 J/mm. The other LED values were distributed inside the best-density process window.

Starting with the reference of the parameter identified by the SLM Solution, the range of LED values examined for the identification of the best conditions of ductility and resistance of the material was chosen. In particular, three different ranges of variation of the LED were selected with increasing amplitudes as the values considered move from the reference value of 0.25 J/mm. According to Table 1, four samples with different process parameters were chosen for the LED range values Δ_{LED2} (ID 6-9) and Δ_{LED3} (ID 10-13), whereas five samples were taken into account for the LED range values Δ_{LED1} (ID 1-5).

The investigated range was selected in accordance with earlier experimental campaigns where significant porosity defects were noted for samples printed outside the range used for this investigation. The process parameters employed in this work, including Laser Power (P), Scanning Speed (v), Hatch Distance (h), Scanning Strategy (s), Building Orientation (b), Layer Thickness (t), and LED, may be seen in Table 1.

Materials Research Proceedings 35 (2023) 241-248 https://doi.org/10.21741/9781644902714-29

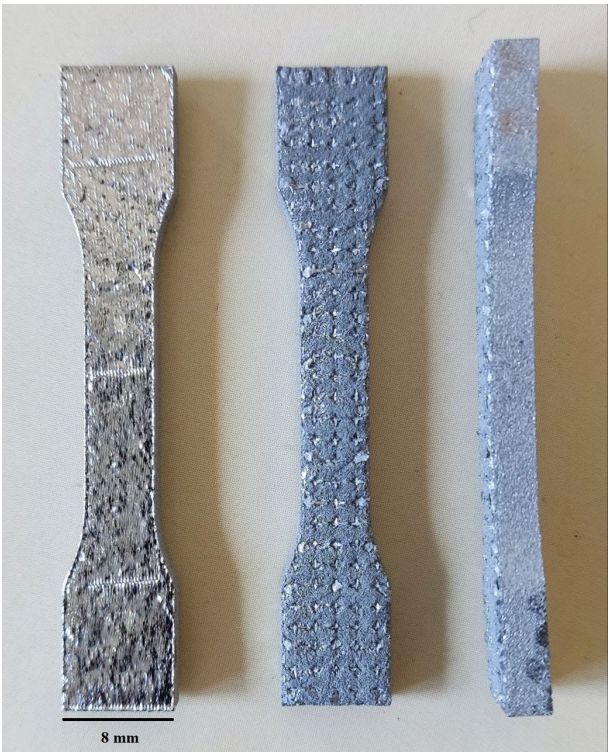

Figure 1. Dog bone samples used for the tensile tests.

Table 1. Process parameters.

ID	P [W]	v [mm/s]	LED [J/mm]	
1	305	1739	0,175	
2	312	1660	0,188	
3	328	1576	0,208	Δ_{LED1}= 0.044
4	334	1552	0,215	
5	338	1541	0,219	
6	348	1506	0,231	
7	351	1516	0,232	Δ_{LED2}= 0.016
8	365	1504	0,243	
9	366	1483	0,247	
10	380	1520	0,250	
11	373	1491	0,250	Δ_{LED3}= 0.008
12	377	1502	0,251	
13	378	1463	0,258	

On a Galdabini Sun 5, quasi-static tensile tests at a rate of 1 mm/min were performed to assess the mechanical behavior of the samples in terms of ultimate tensile strength (UTS) and elongation to failure (ETF). Printed dog bone specimens (Figure 1) with a 5mm × 3mm section were used for the tensile tests as a reduction of the ASTM E8 standard. Archimedes technique was used to estimate relative density, and KERN balance with 0.001g accuracy was used to weigh the samples in air and water.

Materials Research Proceedings 35 (2023) 241-248 https://doi.org/10.21741/9781644902714-29

The reference density value for the Ti6Al4V alloy was considered equal to 4.43 g/cm^3. Furthermore, optical microscope (OM) inspections were carried out to examine fracture surfaces.

For the above analysis, the extent of the fracture propagation surface (A), in the specimens subjected to tensile stress, was measured by means of proper image analysis software.
The materials capacity to absorb energy before failing was also studied in order to identify the optimal material properties suitable for hybrid metal forming processes. The product of the UTS and ETF values can be used to measure the aforementioned factor.

Results and discussion

In order to provide a process window for the hybrid manufacturing process, a preliminary research on the impact of LED on the mechanical behavior of Ti6Al4V parts produced by L-PBF was reviewed in this work. To do this, tensile tests were conducted on each specimen, which were also weighted to determine the relative density. The results were then compared to the mechanical properties, such as UTS and ETF, that had been determined.

Tensile Strength and Elongation to Failure

Regarding the material's tensile strength and elongation, the results of the tensile tests measured in terms of UTS and ETF, show three distinct patterns, unique for each ΔLED range identified, namely Δ_{LED1}, Δ_{LED2}, and Δ_{LED3}. As can be seen from Figure 2, the UTS values exhibit a decreasing trend in the Δ_{LED1} range, a curved trend with a relative maximum in the Δ_{LED2} range, and an almost constant trend in the Δ_{LED3} range.

The ETF trends, on the other hand, display a growing trend in the Δ_{LED1} range, a curved trend with a relative minimum point in the interval Δ_{LED2}, and a nearly constant trend in the interval Δ_{LED3}. Also, it should be observed that from the specimens ID1 to ID13, both the LED and the laser power values increase.

According to the observed trends, the effect of the scanning speed prevails on that one of the laser power for LED values that deviate more from the optimal value recommended for printing (0.25 J/mm). It follows that for high scanning speeds, even when laser power and LED value rise, causes a refinement of the material structure, increasing its mechanical strength at the expense of ductility. A distinct mechanism which results in an increase in mechanical strength and a loss in ductility characteristics is shown when the laser power is increased. This transition zone is seen in the Δ_{LED2} range, where the effect of the scanning speed still predominates. With the activation of more intense heat fluxes that affect the martensite formation mechanism, the material also starts to strengthen in the previously mentioned LED range.

High laser power levels in the range Δ_{LED3} result in the stabilization of the material's strengthening process linked to heat fluxes, deactivating the refining phenomena carried on by the changes in scanning speed. In fact, it is found that in this range, both the material's ductility and mechanical strength follow a nearly constant trend.

Materials Research Proceedings 35 (2023) 241-248 https://doi.org/10.21741/9781644902714-29

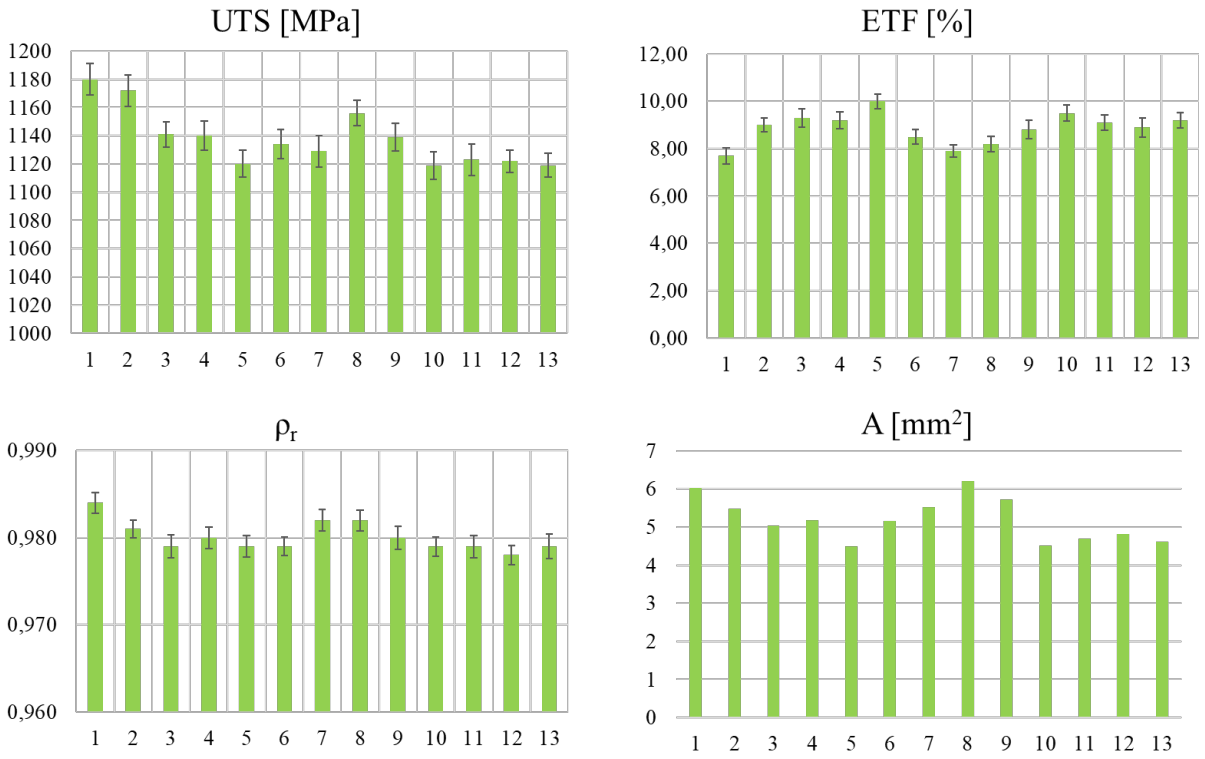

Figure 2. In this figure are shown the results obtained from the tensile tests (UTS, ETF), density measurement (ρ_r), and the fracture surface analysis (A).

The ID 1 sample, which is characterized by the lowest LED and laser power values, showed the best mechanical strength value and the lowest ductility values.

Table 2. Values of UTS×ETF and relative density.

ID	UTS×ETF	ρ_r [%]
1	9086	98,4%
2	10548	98,1%
3	10611	97,9%
4	10488	98,0%
5	11200	97,9%
6	9639	97,9%
7	8919	98,2%
8	9479	98,2%
9	10023	98,0%
10	10631	97,9%
11	10219	97,9%
12	9986	97,8%
13	10295	97,9%

The evaluations conducted in the three ΔLEDs revealed that, in terms of the material capacity to absorb energy before breaking, the best compromise between material strength and ductility

Materials Research Proceedings 35 (2023) 241-248 https://doi.org/10.21741/9781644902714-29

was found not so much at the LED values that are optimal for the printing process but rather at the upper end of the ΔLED1 range, i.e. for the process parameters that characterize sample ID5. The value of the index of the material's ability to absorb energy before failure is displayed for all samples in Table 2 above.

By measuring the size of the fracture propagation area in the necking section, image analysis (Figure 3) was used to analyze the fracture surfaces of the tensile tested specimens. The pattern discovered supports previous tensile strength observations. The image analysis for all the samples (ID1-ID13) is displayed in Figure 3.

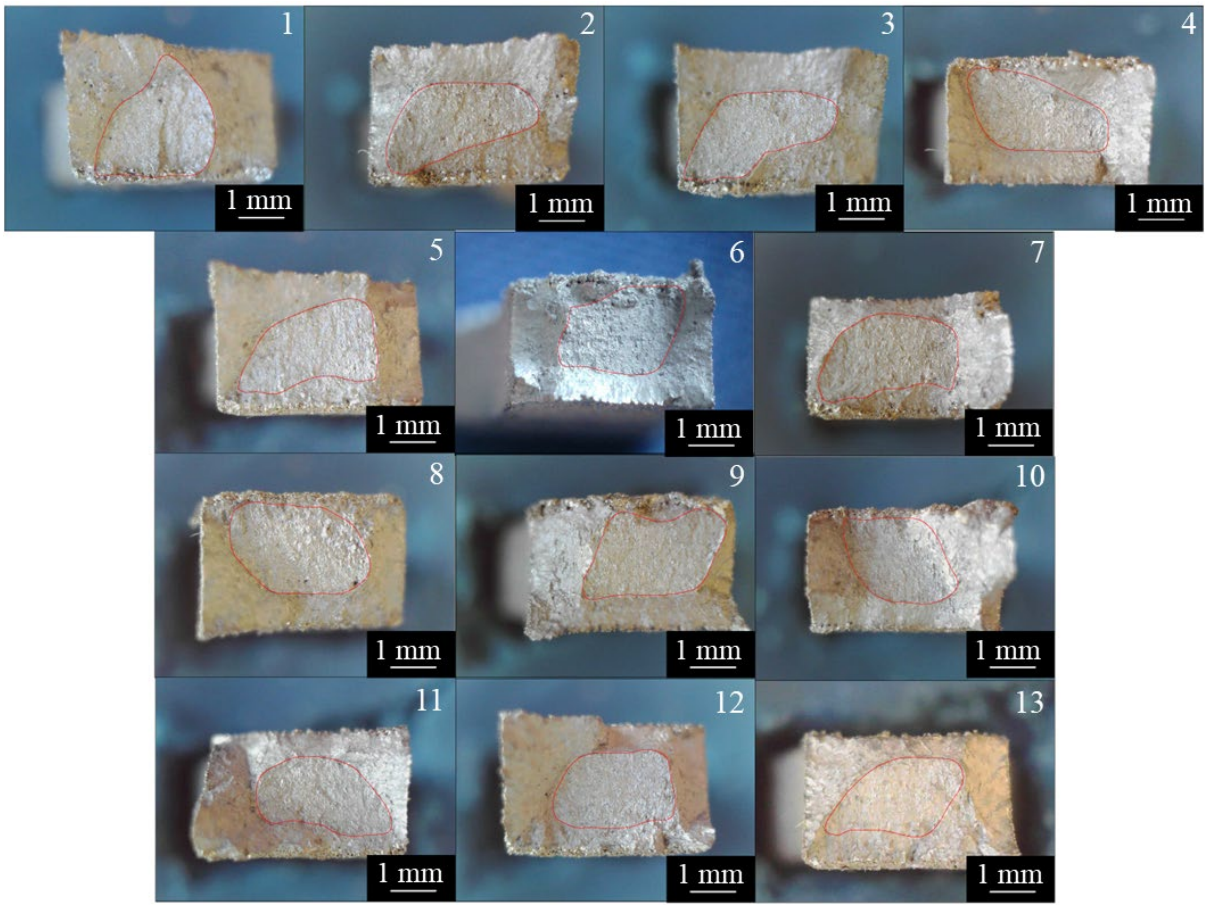

Figure 3. Surface fracture images for all the samples. The fracture propagation area is indicated with a red line.

Relative density

It should be observed that the material's relative density exhibits the same patterns as those required for tensile strength, leading to comparable properties in the three LED range values. The specimen's porosity is caused by a variety of phenomena. The influence of the scanning speed predominates for samples from ID1 to ID5, meaning that less active kinetics of the material in the molten state leads to a higher presence of trapped gas porosity.

The findings from the density measurement are presented in Figure 2. The influence of the kinetics of the material in the molten state, that determines the presence of gas porosity, is still seen in the trend for the samples ID6 to ID9. A stabilization of the material porosity is seen for samples ID10 to ID13. When the laser power is larger than 370 W, the formation of gas porosity is more related on the quantity of the melted material during the scanning phase rather than to the kinetics of the material in the molten state. As a result, the porosity level has stabilized.

Conclusions

Tensile tests, fracture surface analysis, and density measurements were performed in order to investigate the impact of the LED on the mechanical behavior of printed Ti6Al4V parts. The outcomes of this investigation can be used to identify the proper process parameters for the hybrid manufacturing process. The following is a summary of the key findings:

- For high scanning speeds, there is a refinement of the material structure that increases the mechanical strength at the expense of ductility, even when the laser power and the LED value increase.
- There is a process parameter transition zone in which material strengthening is linked to the activation of more severe heat fluxes that affect the martensite production mechanism.
- Increased laser power values stabilize the material-strengthening mechanism connected to heat fluxes, deactivating the refining phenomena caused by varying scanning speeds.
- The best compromise between material strength and ductility was obtained at the upper end of the Δ_{LED1} range, rather than at the optimum LED values for the printing process.
- The relative density of the material follows the same trends as those reported for the tensile strength. The specimen's porosity is also affected by several phenomena. For laser power values higher than 370 W, a stabilization of the material porosity occurs. The onset of gas porosity is more dependent on the amount of molten material than on the kinetics of the molten material.

References

[1] A. Schaub, B. Ahuja, L. Butzhammer, J. Osterziel, M. Schmidt, and M. Merklein, Additive manufacturing of functional elements on sheet metal, Phys. Procedia, 83 (2016) 797–807. https://doi.org/10.1016/j.phpro.2016.08.082

[2] M. D. Bambach, M. Bambach, A. Sviridov, and S. Weiss, New process chains involving additive manufacturing and metal forming - A chance for saving energy?, Procedia Eng., 207 (2017) 1176–1181. https://doi.org/10.1016/j.proeng.2017.10.1049

[3] J. M. Flynn, A. Shokrani, S. T. Newman, and V. Dhokia, Hybrid additive and subtractive machine tools - Research and industrial developments, Int. J. Mach. Tools Manuf., 101 (2016) 79–101. https://doi.org/10.1016/j.ijmachtools.2015.11.007

[4] M. Hirtler, A. Jedynak, B. Sydow, A. Sviridov, and M. Bambach, A study on the mechanical properties of hybrid parts manufactured by forging and wire arc additive manufacturing, Procedia Manuf., 47 (2020) 1141–1148. https://doi.org/10.1016/j.promfg.2020.04.136

[5] M. Merklein, R. Schulte, and T. Papke, An innovative process combination of additive manufacturing and sheet bulk metal forming for manufacturing a functional hybrid part, J. Mater. Process. Technol., 291 (2021) 117032. https://doi.org/10.1016/j.jmatprotec.2020.117032

[6] M. Bambach, I. Sizova, B. Sydow, S. Hemes, and F. Meiners, Hybrid manufacturing of components from Ti-6Al-4V by metal forming and wire-arc additive manufacturing, J. Mater. Process. Technol., 282 (2020) 116689. https://doi.org/10.1016/j.jmatprotec.2020.116689

[7] T. Pasang et al., Directionally-Dependent Mechanical Properties of Ti6Al4V, Materials (Basel)., 14 (2021) 13:3603, doi: https://doi.org/10.3390/ ma14133603

[8] D. Wang, W. Dou, and Y. Yang, Research on selective laser melting of Ti6Al4V: Surface morphologies, optimized processing zone, and ductility improvement mechanism, Metals (Basel)., 8 (2018) 7:471. https://doi.org/10.3390/met8070471

[9] A. Moridi, A. G. Demir, L. Caprio, A. J. Hart, B. Previtali, and B. M. Colosimo, Deformation and failure mechanisms of Ti–6Al–4V as built by selective laser melting, Mater. Sci. Eng. A, 768 (2019) 0–26. https://doi.org/10.1016/j.msea.2019.138456

[10] J. Liu et al., Achieving Ti6Al4V alloys with both high strength and ductility via selective laser melting, Mater. Sci. Eng. A, 766 (2019) 138319. https://doi.org/10.1016/j.msea.2019.138319

[11] D. Palmeri, G. Buffa, G. Pollara, and L. Fratini, The Effect of Building Direction on Microstructure and Microhardness during Selective Laser Melting of Ti6Al4V Titanium Alloy, J. Mater. Eng. Perform., (2021). https://doi.org/10.1007/s11665-021-06039-x

[12] D. Palmeri, G. Buffa, G. Pollara, and L. Fratini, Sample building orientation effect on porosity and mechanical properties in Selective Laser Melting of Ti6Al4V titanium alloy, Mater. Sci. Eng. A, 830 (2022) 142306. https://doi.org/10.1016/j.msea.2021.142306